Analytical determination of the local oxygen structure around Cr^{3+} in SnO_2 rutile-type crystals by use of electron paramagnetic resonance

H. Hikita
Laboratory of Physics, Meikai University, Urayasu, Chiba, Japan

K. Takeda
Electro-Chemical and Cancer Institute, Kokuryo, Chofu, Tokyo, Japan

Y. Kimura
Department of Physics, Faculty of Science, Tokai University, Hiratuka, Kanagawa, Japan
(Received 10 August 1992)

The origin of two distinct electron paramagnetic resonance (EPR) spectra observed in Cr-doped SnO_2 crystals, i.e., $(EPR)_I$ and $(EPR)_{II}$, was investigated using the superposition model specifically developed for rutile-type crystals. Analytical results suggest that these spectra are due to the substitutional Cr^{3+} ions having a unique structure with respect to its local surrounding oxygen atoms. The $(EPR)_I$ spectrum showed that the four nearest-neighbor oxygen atoms on the (110) plane have moved from normal sites toward the Cr^{3+} ion by 0.072 Å (3.5%) as a result of a reduction in the metal ionic radius. The $(EPR)_{II}$ spectrum showed the Cr^{3+} ion to be coupled with the vacancy of the two nearest-neighbor oxygen atoms on the [110] axis. In this case, the ratio of spin-Hamiltonian parameters takes the form $E/D=-\cos 2\alpha$ from the superposition model, where α is the angle between the [001] axis and the cation-ligand bonding axis in (110) plane. The theoretical value $E/D=-0.205$ was obtained from this simple relation, and was in good agreement with the experimental values.

I. INTRODUCTION

SnO_2 is a transparent n-type semiconductor with a wide band gap. It has been considered that its electric conductivity originates from a nonstoichiometric structure containing oxygen vacancies, interstitial Sn ions, or other native defects which form shallow donor centers providing many conduction electrons.[1-7] These phenomena are also found in several excess-type oxide semiconductors such as TiO_2 or ZnO.[2] Although oxygen vacancies were previously suggested to be the most predominate native defect using electrical conductivity temperature-dependent measurements,[7] the nonstoichiometric structure of SnO_2 crystals has not yet been fully elucidated.

Application of electron paramagnetic resonance (EPR) to Cr^{3+}-doped SnO_2 crystals has shown two distinct spectra, i.e., $(EPR)_I$ and $(EPR)_{II}$.[8-11] In addition, an inclusive spectrum $(EPR)_{III}$ was found in as-grown crystals.[12] The angular dependence of these spectra, $(EPR)_I$, $(EPR)_{II}$, and $(EPR)_{III}$, are shown in Fig. 1. The origin of the spectrum $(EPR)_I$ is believed to represent the effect of substitutional Cr^{3+} ions,[9-11] whereas $(EPR)_{II}$ has been considered to be due to interstitial ones.[9,10] We previously showed, using an analysis of the line intensity ratio of the superhyperfine structure of the Sn ion, that $(EPR)_{II}$, like $(EPR)_I$, is attributed to a Cr^{3+} ion located at a substitutional site, rather than at an interstitial site.[10] The difference between $(EPR)_I$ and $(EPR)_{II}$ may arise from a particular defect occurring near the Cr ions in SnO_2 crystals, yet this phenomenon has not been clarified.

An analytical tool was developed to determine the local structure of a crystal's paramagnetic ion from EPR data, i.e., the superposition model.[13-23] This model was originally introduced to analyze spin-Hamiltonian parameters of S-state ions in insulators,[3,14] and assumes these parameters can be described by the individual con-

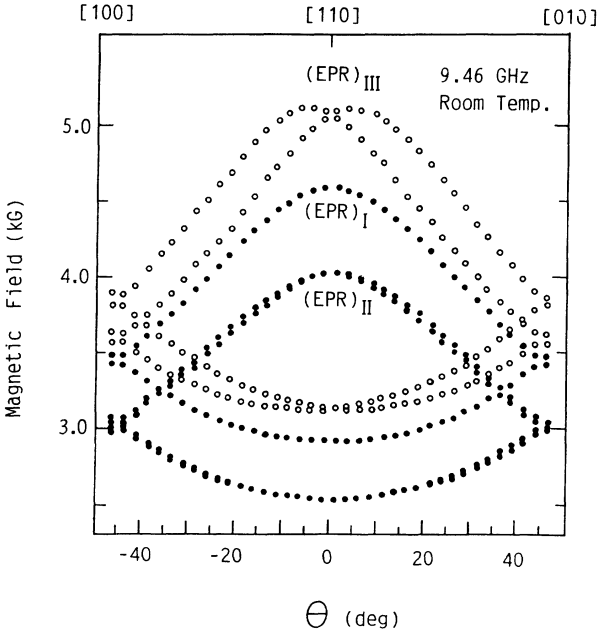

FIG. 1. Angular dependence of EPR spectra of a Cr^{3+}-doped SnO_2 crystal in the (001) plane.

tributions of each nearest-neighbor ligand ion to the paramagnetic ion. The spin-Hamiltonian parameters therefore allow a correlation to be established with the position of the ligand ions; hence enabling the superposition model to be successfully applied to the vacancy free or vacancy associated centers in the perovskite oxides[15–18] and fluorides.[19–22] Consequently, detailed information on the local surroundings of the sixfold coordinated paramagnetic ions has been obtained. It should be noted, however, that only limited research has been directed at using this model to study rutile-type crystals. Recently we proposed the superposition model of Cr^{3+} in such crystals.[24] The present study analytically investigates the origin of the $(EPR)_I$ and $(EPR)_{II}$ spectra using the superposition model which is specifically developed for Cr^{3+} ions in rutile-type crystals.

II. SUPERPOSITION MODEL OF Cr^{3+} IN RUTILE-TYPE CRYSTALS

The superposition model[13–17] assumes that the spin-Hamiltonian parameter b_n^m can be expressed as a superposition of a single ligand contribution, i.e.,

$$b_n^m = \sum_i \bar{b}_n(R_i) K_n^m(\theta_i,\phi_i) , \tag{1}$$

where (R_i,θ_i,ϕ_i) is the polar coordinate for the ith ligand ion, $\bar{b}_n(R_i)$ is an intrinsic parameter which is a function of the metal-ligand distance R_i, and $K_n^m(\theta_i,\phi_i)$ is a spherical harmonic function of polar angles. To calculate the spin-Hamiltonian parameter b_n^m the distance between the metal and ligand must be obtained.

Figure 2 schematically shows the structure of a rutile-type crystal, where the cations have six octahedrally located O^{2-} ions giving a rhombic distortion belonging to point symmetry D_{2h}. The [110] axis of the crystal is chosen as the Z axis and the [001] axis is chosen as the X axis. The positions of the nearest-neighbor oxygens on the Z axis "O_z" have a different symmetry from that of the nearest-neighbor oxygens on the XY plane "O_{xy}." The crystallographic data for rutile-type TiO_2, GeO_2, and SnO_2 were determined by Baur[25] and are summarized in Table I. The parameter α represents the angle between the X axis and the bonding axis of O_{xy}. In rutile-type crystals the host ion is replaced by a Cr ion.

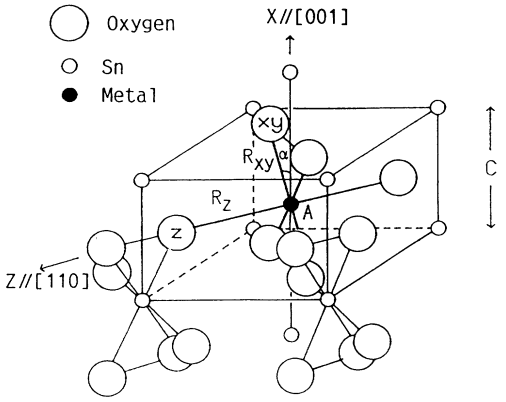

FIG. 2. Crystal structure of rutile-type crystal. The position "A" is a metal ion and the oxygen atoms are represented by large circles. The nearest-neighbor oxygen atoms on the Z axis are annoted as "O_z" and ones on the XY plane as "O_{xy}."

The spin-Hamiltonian of a Cr ion with $S=\frac{3}{2}$ in rutile-type crystals is conventionally written as

$$\mathcal{H}=\beta H\cdot g\cdot S+D[S_z^2-\tfrac{1}{3}S(S+1)]+E(S_x^2-S_y^2) , \tag{2}$$

where the x, y, and z axes are the paramagnetic principal axes and the hyperfine interaction with the Cr^{53} nuclei is neglected. The spin-Hamiltonian parameters D and E for TiO_2:Cr^{3+},[26,27] TiO_2:Mn^{4+},[28] GeO_2:Cr^{3+},[29] and SnO_2:Cr^{3+} (Ref. 11) are listed in Table II. The values of D and E in this table were transformed to the coordinate system shown in Fig. 2.

It is generally known that the ^4F state of Cr ions with d^3 electrons in a rutile-type crystal can be decomposed into seven singlets by the perturbation potential $V(D_{2h})$ with orthorhombic D_{2h} symmetry as shown in the energy diagram of Fig. 3. The probable ground state B_1 is a mixing state of the t_2^3 state and a small portion of the higher t_2e^2 state having the same notation, i.e., $\psi(t_2^3)+\lambda\psi(t_2e^2)$. Such hybridization from a higher state also occurs for d^1 ions as well as for d^3 ions in these crystals.[30–32] Since the mixing parameter λ is dependent on the angle α, the intrinsic parameter of Cr^{3+} in rutile-type crystals with rhombic distortion may have a large anisotropy different from that in cubic crystals. In an octahedron with large anisotropy, even if $R_z=R_{xy}$, the intrinsic parameter $\bar{b}_2(R_z)$ corresponding to O_z would be different from $\bar{b}_2(R_{xy})$ corresponding to O_{xy} in symmetry. As a result, the summation in Eq. (1) of intrinsic parameters for ligand oxygens must be divided into two parts according to the rhombic distortion of the octahedron, i.e., one being the sum for the two O_z atoms on the Z axis and the other the sum for the four O_{xy} atoms on the XY plane. The spin-Hamiltonian parameters D and E in Eq. (2) can therefore be written for rutile-type crystals as

$$D=b_2^0=2\bar{b}_2(R_z)-2\bar{b}_2(R_{xy}) , \tag{3}$$

$$E=\tfrac{1}{3}b_2^2=2\bar{b}_2(R_{xy})\cos 2\alpha . \tag{4}$$

The intrinsic parameter $\bar{b}_2(R_z)$ is a function of the distance between the Cr^{3+} ion and O_z, while $\bar{b}_2(R_{xy})$ is a function of the distance between the Cr^{3+} ion and O_{xy}. When D and E in Eqs. (3) and (4) are set equal to zero, this corresponds to cubic symmetry without the Jahn-Teller effect, where $R_z=R_{xy}$ and $\alpha=45°$.

Müller *et al.*[16–18] showed that for Cr^{3+} ions in cubic

TABLE I. Crystallographic data of TiO_2, GeO_2, and SnO_2. R_z is the distance between the cation and O_z, and R_{xy} is the distance between the cation and O_{xy}. α is an angle, less than 45°, between the X axis and the cation-O_{xy} bonding axis in the XY plane.

	a (Å)	c (Å)	R_z (Å)	R_{xy} (Å)	α (°)
TiO_2	4.594	2.959	1.988	1.944	40.44
GeO_2	4.395	2.860	1.91	1.87	39.9
SnO_2	4.737	3.185	2.056	2.052	39.09

TABLE II. Spin-Hamiltonian parameters of Cr^{3+} and Mn^{4+} in rutile-type crystals. The values for $|D|$ and $|E|$ are in units of cm^{-1}.

	g	$\|D\|$	$\|E\|$	Ref.
TiO_2:Cr^{3+}	1.97	0.680	0.140[b]	26,27
TiO_2:Mn^{4+}	1.9983	0.400	0.139[a]	28
GeO_2:Cr^{3+}	1.980	0.634	0.137[a]	29
SnO_2:Cr^{3+}				
$(EPR)_I$	1.976	0.651	0.174[b]	11
$(EPR)_{II}$	1.975	0.703	0.146[b]	11

[a] $E/D<0$ for all crystals.
[b] $D<0$.

crystals, the intrinsic parameter $\bar{b}_2(R)$ is represented by a Lennard-Jones-type function having a two-term power law with constants A and B given as

$$\bar{b}_2(R)=-A\left[\frac{R_0}{R}\right]^n+B\left[\frac{R_0}{R}\right]^m, \tag{5}$$

where R_0 is a reference length and R is the distance between the metal and ligand. However, Eq. (5) must be modified for rutile-type crystals because of the large rhombic distortion due to O_z and O_{xy} having nonsymmetric sites with respect to the metal ion. Equation (5) should then be rewritten as

$$\bar{b}_2(R_z)=-A_1\left[\frac{R_0}{R_z}\right]^n+B_1\left[\frac{R_0}{R_z}\right]^m, \tag{6}$$

$$\bar{b}_2(R_{xy})=-A_2\left[\frac{R_0'}{R_{xy}}\right]^n+B_2\left[\frac{R_0'}{R_{xy}}\right]^m, \tag{7}$$

where A_1 and B_1 denote the constants for $\bar{b}_2(R_z)$, and

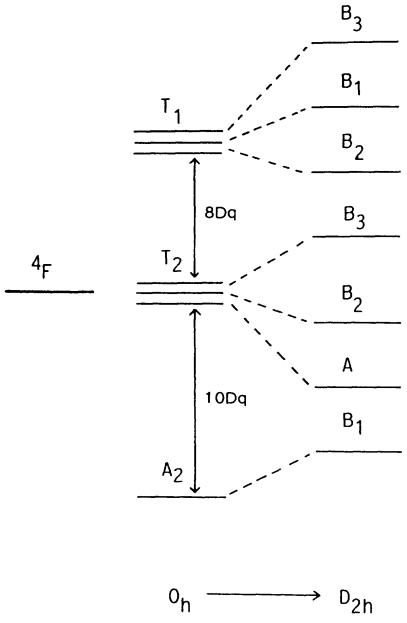

FIG. 3. Schematic energy level diagram for a Cr^3 ion in a rutile-type crystal.

TABLE III. Calculated superposition model parameters for Cr^{3+} in rutile-type crystals and those from the cubic crystals $SrTiO_3$ and MgO (Ref. 16).

	Rutile type		$SrTiO_3$	MgO
	(z)	(xy)		
R_0 (Å)	2.056	2.052	1.952	2.101
R_m (Å)	2.003	1.932	1.967	2.102
A (cm^{-1})	−0.375	−1.074	−10.6	−8.8
B (cm^{-1})	−0.278	−0.717	−8.2	−6.5
n	12	12	~10	~10
m	15	15	~13	~13

A_2 and B_2 for $\bar{b}_2(R_{xy})$. R_0 and R_0' are, respectively, set equal to the reference length of 2.056 and 2.052 Å from the SnO_2 crystal. The exponents n and m are on the order of 10, and the constraint $m-n=3$ is imposed.[16] The intrinsic parameters in Eqs. (6) and (7) have extremal values at

$$R_m=R_0\left[\frac{mB_1}{nA_1}\right]^{1/(m-n)} \tag{8}$$

$$R_m'=R_0'\left[\frac{mB_2}{nA_2}\right]^{1/(m-n)}, \tag{9}$$

where the distance R_m on the Z axis gives the extremal value of $\bar{b}_2(R_z)$ and R_m' on the XY plane gives those for $\bar{b}_2(R_{xy})$.

The experimental values of $\bar{b}_2(R_z)$ and $\bar{b}_2(R_{xy})$ for rutile-type crystals were obtained from Eqs. (3) and (4) using the spin-Hamiltonian parameters D and E in Table II. The constants A_1, B_1, A_2, B_2, n, and m in Eqs. (6) and (7) were determined from the intrinsic parameters of rutile-type crystals GeO_2 and TiO_2. Table III lists the calculated values of these constants, and for reference the constants for the cubic crystals $SrTiO_3$ and MgO are shown.[16] Notice that these constants of rutile-type crystals are about $\frac{1}{10}$ those of cubic crystals. In addition, A_1

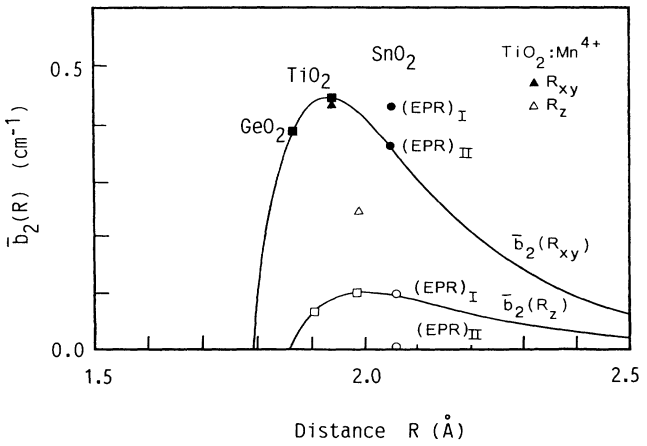

FIG. 4. $\bar{b}_2(R_z)$ and $\bar{b}_2(R_{xy})$ vs distance. Experimental values of $\bar{b}_2(R_z)$ and $\bar{b}_2(R_{xy})$ of GeO_2:Cr^{3+}, TiO_2:Cr^{3+}, and SnO_2:Cr^{3+} are also indicated.

and B_1 for R_z are approximately three times smaller than A_2 and B_2 for R_{xy}. Figure 4 shows curves of the intrinsic parameters using these calculated constants as a function of the distance between the Cr^{3+} ion and oxygen atom. The experimental values of $\bar{b}_2(R_z)$ and $\bar{b}_2(R_{xy})$ obtained from the D and E in Table II are also shown. It should be noted that the intrinsic parameter for R_z of TiO_2:Mn^{4+} is twice as large as that of Cr^{3+} in rutile-type crystals, possibly a result of the interaction of Mn^{4+} with the oxygen atom on the [110] axis being different from the interaction of Cr^{3+} with oxygen atoms.

III. ANALYSIS OF THE $(EPR)_I$ AND $(EPR)_{II}$ SPECTRA

A. $(EPR)_I$

The experimental intrinsic parameter for R_z from $(EPR)_I$ correlates well with the theoretical $\bar{b}_2(R_z)$ function as shown in Fig. 4. In contrast, however, the corresponding value for R_{xy} does not fit the $\bar{b}_2(R_{xy})$ function. This subsequently indicates that the O_{xy} atoms moved from their normal sites toward the central Cr^{3+} ion while the O_z atoms have remained stationary. If the displaced oxygen atoms leave the crystal axes, then the magnetic principal axes would shift from these axes. However, the magnetic principal axes of $(EPR)_I$ coincide with the orientation of the crystal axes of the octahedron; hence the displaced O_{xy} atoms would lie on the Cr-O_{xy} bonding axis. The distance from the Cr ion to the O_z and O_{xy} atoms is, respectively, expressed as

$$R_z = R_0 \ , \tag{10}$$

$$R_{xy} = R_0' + \Delta_{xy} \ , \tag{11}$$

where Δ_{xy} is the displacement of the O_{xy} atoms from the reference length R_0' on the Cr-O_{xy} bonding axis. The spin-Hamiltonian parameters D and E in Eqs. (3) and (4) can then be represented as a function of Δ_{xy}. It is convenient to use the ratio Δ_{xy}/R_0' in Eqs. (6) and (7) to represent the displacement from the normal site. Figure 5 shows the variation of the spin-Hamiltonian parameters D and E in Eqs. (3) and (4) versus Δ_{xy}/R_0', where two points on the D and E curves, i.e., $\Delta_{xy}/R_0' = -0.078$ and -0.035, corresponded with the experimentally obtained $(EPR)_I$ parameters. As shown by Table IV, the radius of Cr^{3+}, $R(Cr^{3+})$, is 0.08 Å less than that of Sn^{4+}, $R(Sn^{4+})$. At $\Delta_{xy}/R_0' = -0.078$, $\Delta_{xy} = -0.16$ Å; thus, the displacement of the O_{xy} atoms towards the central Cr^{3+} ion is much larger than the reduction of the metal-ionic radius $[R(Cr^{3+}) - R(Sn^{4+}) = -0.08$ Å] and electrons in the outer shell of O^{2-} would then overlap onto the Cr^{3+} ion. Such a large displacement in O_{xy} atoms can obviously be excluded. On the other hand, when $\Delta_{xy}/R_0' = -0.035$, then $\Delta_{xy} = -0.072$ Å, being in good agreement with

$$\frac{R(Cr^{3+}) - R(Sn^{4+})}{R_0'} = -0.039 \ . \tag{12}$$

In this case the displacement of the O_{xy} atoms corresponds to the reduction of the metal-ionic radius. The distance between the O_{xy} atoms and the Cr ion in the XY

TABLE IV. Ion radii of Sn^{4+}, Ti^{4+}, Ge^{4+}, Cr^{3+}, and O^{2-}. Units of Å are used.

Sn^{4+}	Ti^{4+}	Ge^{4+}	Cr^{3+}	O^{2-}
0.84	0.77	0.69	0.76	1.22

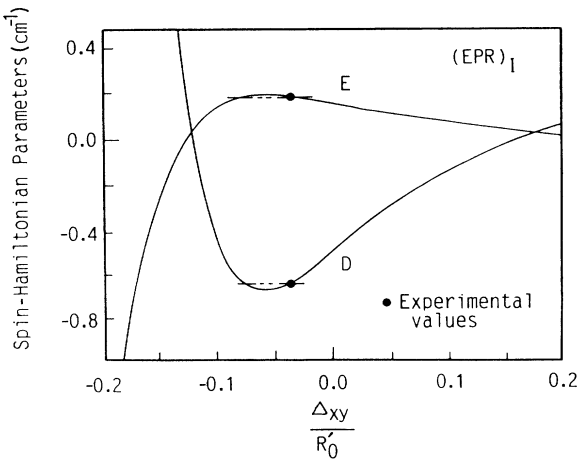

FIG. 5. Spin-Hamiltonian parameters vs Δ_{xy}/R' when the two nearest-neighbor oxygen atoms on the Z axis are located at their normal sites. Experimental values of D and E for $(EPR)_I$ are also indicated.

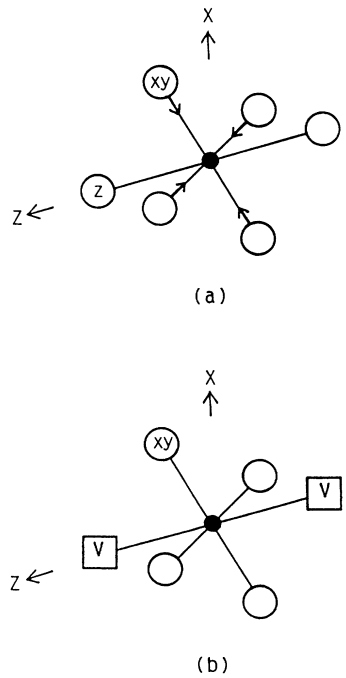

FIG. 6. Local structure of oxygen atoms around a Cr^{3+} ion for $(EPR)_I$ and $(EPR)_{II}$. (a) Representation of $(EPR)_I$ in which the nearest-neighbor oxygen atoms on the XY plane move toward the Cr^{3+} ion in the octahedron. (b) Representation of $(EPR)_{II}$ in which the nearest-neighbor oxygen atoms on the Z axis are vacant.

plane would decrease by 0.072 Å, or 3.5%, in the direction of the Cr-O_{xy} bond due to the small ion radius of Cr^{3+}, i.e., O_{xy} atoms are 1.980 Å away from Cr^{3+} on the XY plane and O_z atoms are at their normal sites as shown in Fig. 6(a).

If the presented superposition model was incorrect, then the value Δ_{xy}/R_0' for the experimental values of D would not correlate with one for the experimental E. Experimental data of D and E, shown in Fig. 5, however, show good agreement at the same ratio Δ_{xy}/R_0'. It is therefore concluded that the spin-Hamiltonian parameters D and E for $(EPR)_I$ are only a function of Δ_{xy}/R_0' at a constant R_z.

B. $(EPR)_{II}$

As shown in Fig. 4, the experimental intrinsic parameter $\bar{b}_2(R_z)$ for $(EPR)_{II}$ is near zero, thus suggesting it is negligible, and thereby allowing Eqs. (3) and (4) to be rewritten as

$$D_v = -2\bar{b}_2(R_{xy}) , \tag{13}$$

$$E_v = 2\bar{b}_2(R_{xy})\cos 2\alpha , \tag{14}$$

where D_v and E_v denote the theoretical spin-Hamiltonian parameters for $\bar{b}_2(R_z)=0$. Note, if R_z in Eq. (6) goes to infinity, then the intrinsic parameter for R_z approaches zero. Therefore, Eqs. (13) and (14) represent the vacancies of two O_z atoms [Fig. 6(b)]. The spin-Hamiltonian parameters D_v and E_v having the two O_z vacancies are shown in Fig. 7. For reference, parameter D from Eq. (3) having two O_z atoms at $R_0=R_z$ is also shown (see Fig. 5). On the D_v and E_v curves, two points, i.e., $\Delta_{xy}/R_0'=-0.096$ and 0, corresponded with the experimentally obtained D and E values, respectively. The experimental values of D and E are particularly shown as D_{exp} and E_{exp} at $\Delta_{xy}/R_0'=0$, respectively. As indicated in Fig. 7, D_{exp} does not agree with D from Eq. (3). When

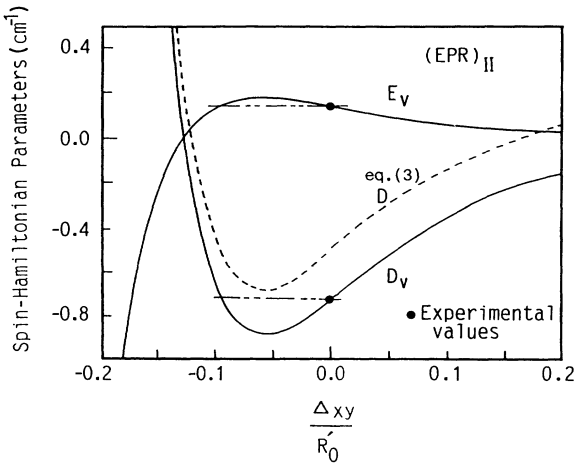

FIG. 7. Spin-Hamiltonian parameters vs Δ_{xy}/R' when the two nearest-neighbor oxygen atoms are vacant. The spin-Hamiltonian parameter D from Eq. (3) is as shown. Experimental values of D and E, i.e., D_{exp} and E_{exp}, are also indicated by solid circles.

$\Delta_{xy}/R_0'=-0.096$, then $\Delta_{xy}=-0.20$ Å; and the displacement of the O_{xy} atoms is too large for the Cr^{3+} ion to easily replace the Sn^{4+} one. It therefore seems reasonable that

$$\Delta_{xy}/R_0'=0, \quad \Delta_{xy}=0 .$$

This implies that the four O_{xy} atoms remain at their normal sites and that the two O_z atoms are vacant as schematically shown in Fig. 6(b). The vacant O_z atoms in $(EPR)_{II}$ would then compensate for the trivalent ion charges if the O_{xy} atoms stayed in their normal sites.

From Eqs. (13) and (14), a simple theoretical ratio for the spin-Hamiltonian parameters can be obtained as follows:

$$\frac{E_v}{D_v} = -\cos 2\alpha , \tag{15}$$

where the ratio E_v/D_v depends only on the angle α. A comparison of the theoretical E_v/D_v using the value of $\alpha=39.09°$ from Table I and the experimental value E_{exp}/D_{exp} from $(EPR)_{II}$ shows good agreement, i.e.,

$$E_v/D_v=-0.205, \quad E_{exp}/D_{exp}=-0.208 .$$

The ratio E_{exp}/D_{exp} can also be directly determined from the experiment of the angular dependence of $(EPR)_{II}$ by

$$\frac{E_{exp}}{D_{exp}} = \frac{1-3\cos^2\theta}{3\sin^2\theta} , \tag{16}$$

where θ is the angle at which the allowed and forbidden transition energies are equal in the resonance magnetic field on the [001] plane. Equation (16) also provides a means for checking the ratio E_v/D_v using an experimentally obtained value of $\theta=66°$. This large angle is actually located outside Fig. 1. The experimental study for this angle would be published elsewhere by us. By substituting $\theta=66°$ into Eq. (16), the ratio $E_{exp}/D_{exp}=-0.201$ is obtained, a value which correlates well with E_v/D_v in both magnitude and sign.

The spin-Hamiltonian parameters for an interstitial Cr^{3+} ion can be calculated from Eqs. (3) and (4). The conventional SnO_2 lattice constants give $R_z=1.718$ Å, $R_{xy}=2.342$ Å, and $\alpha=47.2°$, with $D=-1.99$ cm^{-1}, $E=-0.02$ cm^{-1}, and $E/D=0.01$. However, it should be noted that these values are significantly different from those of $(EPR)_{II}$, especially the positive sign for the ratio E/D. It is consequently concluded that the $(EPR)_{II}$ spectrum does not apply to the interstitial Cr^{3+} ion, but instead indicates a substitutional Cr^{3+} ion, being consistent with an analysis of the line intensity ratio of the superhyperfine structure.[12]

Hou, Summitt, and Tucker[9] obtained the $(EPR)_{II}$ spectrum for Cr^{3+} in reduced SnO_2 crystals and no $(EPR)_I$ spectrum was observed. Furthermore, in reoxidized crystals the opposite phenomenon occurred. We consider that these phenomena are associated with the existence of oxygen atom vacancies for $(EPR)_{II}$. These vacancies in SnO_2 crystals would be an essential defect in its nonstoichiometry structure. In fact, if many Sn^{4+} ions exist

in SnO_2 crystals which are coupled nonstoichiometry with the two oxygen vacancies on the Z axis, then these Sn^{4+} ions can easily be substituted for by the Cr^{3+} ions.

IV. CONCLUSIONS

The origin of the EPR spectra, $(EPR)_I$ and $(EPR)_{II}$, for Cr-doped SnO_2 crystals was investigated by applying the superposition model specifically developed for Cr^{3+} ions in rutile-type crystals. The results suggested that these spectra originated from the substitutional Cr^{3+} having the different local structure of its surrounding oxygen atoms. The $(EPR)_I$ spectrum showed that the four nearest-neighbor oxygen atoms on the XY plane moved toward the central substitutional Cr^{3+} ion by 0.072 Å (3.5%) in comparison to the normal oxygen octahedron. This decrease of the distance between Cr^{3+} and oxygens corresponds to the reduction in the metal-ionic radius. On the other hand, the $(EPR)_{II}$ spectrum showed the Cr^{3+} ion to be coupled with the vacancy of two nearest-neighbor oxygen atoms on the Z axis. The ratio $E/D = -0.205$ was theoretically obtained from the superposition model, and showed in good agreement with the experimental E/D in both magnitude and sign.

ACKNOWLEDGMENT

This work was supported by the Electro-Chemical and Cancer Institute, Tokyo, Japan.

[1]M. Nagasawa, S. Shionoya, and S. Makishima, Jpn. J. Appl. Phys. **4**, 195 (1965).
[2]M. Nagasawa and S. Shionoya, Jpn. J. Appl. Phys. **10**, 472 (1971).
[3]M. Nagasawa and S. Shionoya, J. Phys. Soc. Jpn. **30**, 1118 (1971).
[4]Z. M. Jarzebski and J. P. Marton, J. Electrochem. Soc. **123**, 199C (1976).
[5]Z. M. Jarzebski and J. P. Marton, J. Electrochem. Soc. **123**, 299C (1976).
[6]Z. M. Jarzebski and J. P. Marton, J. Electrochem. Soc. **123**, 333C (1976).
[7]S. Samson and C. G. Fonstad, J. Appl. Phys. **44**, 4618 (1973).
[8]W. H. From, Phys. Rev. **131**, 961 (1963).
[9]S. L. Hou, R. W. Summitt, and R. F. Tucker, Phys. Rev. **154**, 258 (1967).
[10]W. Rhein, Z. Naturforsch. Teil A **27**, 741 (1972).
[11]H. Hikita, K. Takeda, Y. Kimura, and T. Kurose, J. Phys. Soc. Jpn. **57**, 2529 (1988).
[12]H. Hikita, K. Takeda, and Y. Kimura, Phys. Status Solidi A **119**, 251 (1990).
[13]D. J. Newman and W. Urban, Adv. Phys. **24**, 793 (1975).
[14]D. J. Newman and E. Siegel, J. Phys. C **9**, 4285 (1976).
[15]E. Siegel and K. A. Müller, Phys. Rev. B **20**, 3587 (1979).
[16]K. A. Müller and W. Berlinger, J. Phys. C **16**, 6861 (1983).
[17]K. A. Müller, W. Berlinger, and J. Albers, Phys. Rev. B **32**, 5837 (1985).
[18]K. A. Müller, J. Phys. Soc. Jpn. **55**, 719 (1986).
[19]M. Arakawa, H. Aoki, H. Takeuchi, T. Yosida, and K. Horai, J. Phys. Soc. Jpn. **51**, 2459 (1982).
[20]H. Takeuchi and M. Arakawa, J. Phys. Soc. Jpn. **53**, 376 (1984).
[21]M. Arakawa, H. Ebisu, and H. Takeuchi, J. Phys. Soc. Jpn. **55**, 2853 (1986).
[22]M. Arakawa, H. Ebisu, and H. Takeuchi, J. Phys. Soc. Jpn. **57**, 2801 (1988).
[23]C. Rudowicz, Phys. Rev. B **37**, 27 (1988).
[24]H. Hikita, K. Takeda, and Y. Kimura, Solid State Commun. **74**, 1241 (1990).
[25]W. H. Baur, Acta Crystallogr. **9**, 515 (1956).
[26]H. J. Gerritsen, S. E. Harrison, H. R. Lewis, and J. P. Wittke, Phys. Rev. Lett. **2**, 153 (1959).
[27]H. J. Gerritsen, S. E. Harrison, and H. R. Lewis, J. Appl. Phys. **31**, 1566 (1960).
[28]H. G. Andresen, J. Chem. Phys. **35**, 1090 (1961).
[29]P. P. Madacsi, M. Stapelbroek, and O. R. Gilliam, Phys. Rev. B **9**, 2023 (1974).
[30]C. Kikuchi, I. Chen. W. H. From, and P. W. Dorain, J. Chem. Phys. **42**, 181 (1965).
[31]T. Shimizu, J. Phys. Soc. Jpn. **23**, 848 (1967).
[32]D. P. Madacsi and O. R. Gilliam, Phys. Lett. **41A**, 63 (1972).